Advanced Composite Materials
Publication details, including instructions for authors and subscription information:
http://www.tandfonline.com/loi/tacm20

Effect of the Hole on the Tensile Fatigue Properties of CFRP Laminates

Yeon Soo Lee [a] , Goichi Ben [b] & Se Hwan Lee [c]

[a] School of Information and Mechatronics, Gwangju Institute of Science and Technology 1 Oryong-dong, Buk-gu, Gwangju, 500-712, Korea

[b] Department of Mechanical Engineering, College of Industrial Technology, Nihon University, 1-2-1 Izumi-cho, Narashino-shi, Chiba 275-8575, Japan

[c] The 1st PGM R&D Center, Agency for Defense Development, Jochiwon-gil 462, Yuseong, Daejeon, 305-152, Korea;, Email: sehlee13@gmail.com

Version of record first published: 02 Apr 2012.

To cite this article: Yeon Soo Lee , Goichi Ben & Se Hwan Lee (2009): Effect of the Hole on the Tensile Fatigue Properties of CFRP Laminates, Advanced Composite Materials, 18:1, 43-59

To link to this article: http://dx.doi.org/10.1163/156855109X405290

VSP

Advanced Composite Materials 18 (2009) 43–59

ADVANCED COMPOSITE MATERIALS
www.brill.nl/acm

Effect of the Hole on the Tensile Fatigue Properties of CFRP Laminates

Yeon Soo Lee [a], **Goichi Ben** [b] **and Se Hwan Lee** [c,*]

[a] School of Information and Mechatronics, Gwangju Institute of Science and Technology 1 Oryong-dong, Buk-gu, Gwangju, 500-712, Korea

[b] Department of Mechanical Engineering, College of Industrial Technology, Nihon University, 1-2-1 Izumi-cho, Narashino-shi, Chiba 275-8575, Japan

[c] The 1st PGM R&D Center, Agency for Defense Development, Jochiwon-gil 462, Yuseong, Daejeon, 305-152, Korea

Received 3 June 2008; accepted 29 July 2008

Abstract

The current study assessed the effect of a bolt hole on tensile fatigue properties of CFRP laminates. Two specimens, i.e. $[(0/90)_3]_S$, $[(0/45/90/-45)_2]_S$, were analyzed using a finite element method and were experimentally tested for cases, both with and without a hole, whose diameter corresponded to 0.12 times the specimen width. Delamination positions predicted by a 3-dimensional static finite element analysis were matched well to those observed by an ultrasonic imaging system in the middle of fatigue test. A hole whose diameter corresponds to 0.12 times the specimen width caused the fatigue strength to decrease by 9% and 11% under 5 Hz loading frequency, and by 22% and 25% under 10 Hz loading frequency for $[(0/90)_3]_S$ and $[(0/45/90/-45)_2]_S$, respectively. Because the decrease in sectional area due to the hole was normalized in calculation of the tensile strength, a stress concentration around the hole is believed to induce the strength degradation of fatigue specimens. From the finite element analyses, the stress concentration factor around a hole was expected as 8.8 and 9.5 for $[(0/90)_3]_S$ and $[(0/45/90/-45)_2]_S$, respectively.

Keywords

CFRP (Carbon Fiber Reinforced Plastic), fatigue, strength, bolt hole, finite element analysis, infrared imaging system

1. Introduction

Effects of bolt holes on fatigue properties of carbon fiber reinforced polymer (CFRP) laminates should be considered for mechanical safety of CFRP jointing under cycling load [1–3]. When CFRP laminate composites are used in bridge structures, a laminate must be bolted or pin-jointed to other laminates or other kind of

* To whom correspondence should be addressed. E-mail: sehlee13@gmail.com
Edited by the KSCM

 DOI:10.1163/156855109X405290

structural bodies and is subjected to frequency of 2–12 Hz [4]. A CFRP laminate with a bolt hole can resist less tensile or compressive force than that with no hole because the cross-sectional area decreases due to the hole. Besides the reduced sectional area, stress concentration around the hole may also cause the CFRP to fail under less force [5–7]. In addition, fatigue due to cycling loads may affect the strength of CFRP.

The current study aimed to assess the effect of a bolt hole on the fatigue properties of CFRP laminates. The fatigue properties of CFRP laminates with and without a hole were compared from the point of view of strength and fatigue life. We performed a synthetic method, which included non-contacting measurement of stress by infrared rays, fractographies and a finite element analyses.

2. Materials and Methods

Tests and analyses were designed to assess effects of a hole and cycling loads. Effects of the hole and the fatigue (cycling loads) on tensile strength were evaluated by comparing quasi-static tensile test results and fatigue test results. The effects of the delamination produced by cycling loads and of the hole on the stress concentration factors and the delamination positions were estimated by finite element analyses and were compared with fatigue test results.

2.1. Mechanical Tests

A servo-pulser mechanical testing machine (EHHF-EG200KN-40L, Shimadzu Co., Kyoto, Japan) combined with an infrared imaging measurement system (JTG-8010, Japan Electron Optics Laboratory Co. Ltd) was used to do static and fatigue tests (Fig. 1).

2.1.1. Specimens

CFRP laminates were made by the hot-pressure molding of unidirectional prepregs (TR330E-150S, Mitsubishi Rayon Co. Ltd, Tokyo, Japan). The prepregs were manufactured to have 70% of volume fraction after being cured. For a hot-pressing, the bonding pressure was applied under the pressure of 17 MPa, and heat was supplied during 40 min under 120°C. The CFRP specimens were cut as 200 mm × 25 mm and, specially for the CFRP specimens, a hole of 3 mm in diameter was machined (Fig. 2). For grabbing of the specimens by mechanical fixture, two tabs were made of graphite fiber reinforced plastic (GFRP) (50 mm × 25 mm × 1.5 mm) and were bonded on both surfaces of the specimen with thermoset bond of a film type (AF163-2, 3M Co., MN, USA). Finally, the integrity of the specimens was assessed by scanning to find any structural fault using an ultrasonic detector of a water soak type (SDS-6500R, Krautkramer Japan Co. Ltd, Tokyo, Japan). For each testing condition, at least 5 specimens were used.

2.1.2. Static Tensile Failure Tests

The static tensile strength (S_t) of CFRP specimens was measured under the stroke control of 0.5 mm/min. As basic laminate specimens, three kinds of CFRP lami-

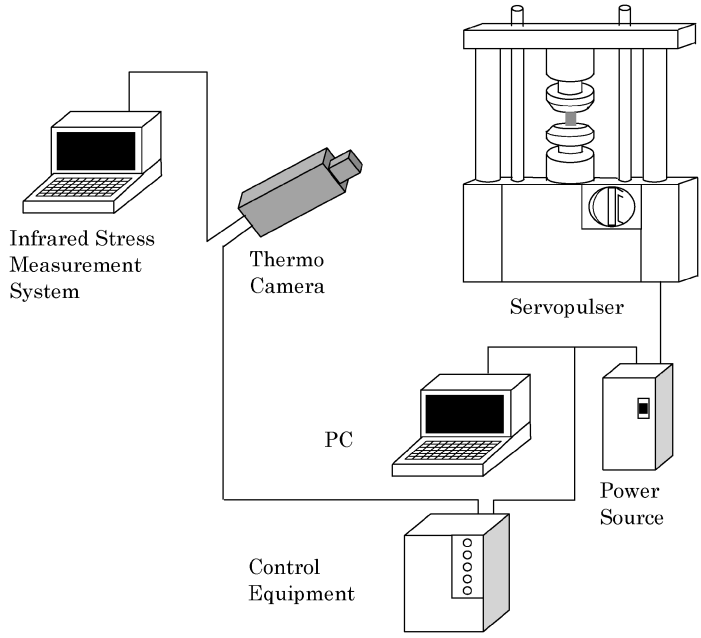

Figure 1. Geometry of the test specimen.

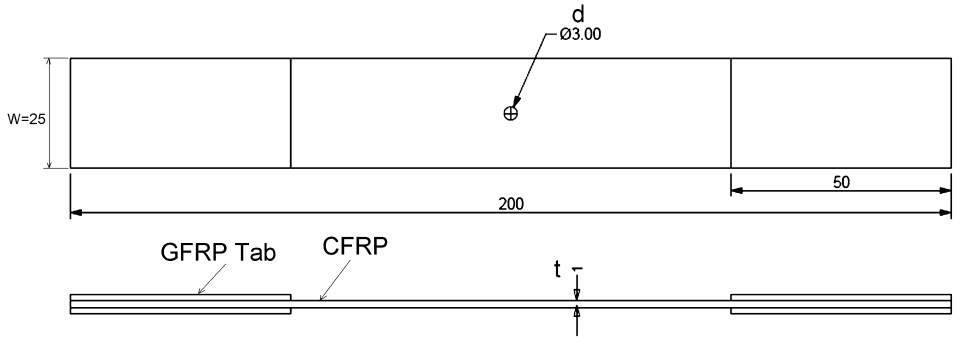

Figure 2. Fatigue testing machine combined with an infrared image system.

nates specimens, namely $[0_8]$, $[90_8]$ and $[(\pm 45)_2]_S$, were tested. Two other kinds of CFRP laminate specimens, namely $[(0/90)_3]_S$ and $[(0/45/90/-45)_2]_S$, were also tested as the main interests of the project. Strengths of CFRP specimens with no hole were calculated by dividing the ultimate failure load by the cross-sectional area perpendicular to loading direction. From the stress–strain curve of the CFRP specimens with no hole, Young's modulus (E) of each specimen was obtained. Strengths (S_t) of CFRP specimens with a hole were represented by the net section stress, which is the ultimate failure load divided by the transverse cross-sectional area excluding the hole area [8]:

$$S_t = \frac{P}{W \times t} \quad \text{with no hole,} \tag{1}$$

$$S_t = \frac{P}{(W-d)\times t} \quad \text{with a hole.} \tag{2}$$

In the equations (1) and (2), W and t denote the width and thickness of the specimen, respectively; t and P denote the diameter of the hole and the failure load in the direction normal to the width direction, respectively.

2.1.3. Fatigue Tests

The specimens for fatigue tests were $[(0/45/90/-45)_2]_S$ and $[(0/90)_3]_S$. The loading conditions of the fatigue tests were determined based on the tensile strength (S_t) of static specimens. The applied maximum stresses (σ_0) for the fatigue tests were specified as ($0.55 \times S_t \sim 0.55 \times S_t$) and ($0.65 \times S_t \sim 0.85 \times S_t$) for $[(0/45/90/-45)_2]_S$ without and with a hole, respectively. They were ($0.75 \times S_t \sim 0.95 \times S_t$) and ($0.99 \times S_t \sim 1.0 \times S_t$) for $[(0/90)_3]_S$ without a hole and with a hole, respectively. The stress ratio (R) was set as 0.1 so that the minimum stress level became $0.1 \times \sigma_0$. The loading frequencies (f) were 5 Hz and 10 Hz. A fracture of a specimen was detected when the displacement rate of loading head is 50 mm/s or the reading of load cell drops at 1000 N/s.

2.1.4. Observation of Delamination Position Using an Ultrasonic Imaging System

In the middle of the fatigue tests, the delamination position was inspected. At the half number of the maximum cycling, which was obtained from the first fatigue test for each type of specimen, fatigue tests from the second specimen of that type of specimen were paused for the inspection of delamination position. For the inspection of delamination position, an ultrasonic detector of a water soak type (SDS-6500R, Krautkramer Japan Co. Ltd, Tokyo, Japan) was used. The ultrasonic inspection system has been widely used to detect delamination area in an inner portion of a CFRP laminate after applying a number of cycling loads or impact loads [9, 10].

2.1.5. In Situ *Stress Distribution Measured by an Infrared Stress Imaging System*

During fatigue tests, the stress distribution image on the surface of a specimen was obtained based on a thermoelastic effect using an infrared imaging system (JTG-8010, Japan Electron Optics Laboratory Co. Ltd, Tokyo, Japan). Infrared inspection systems have been used for the quantitative *in situ* stress measurement of fiber-reinforced plastics [11–14]. An advantage of the infrared thermographic technique is that it can find out the position of the fatigue failure on the specimen [13].

Graphite powders were coated on the surfaces of a specimen to increase the radiation efficacy of the infrared rays. Before loading, the temperature on the surfaces of a specimen was measured by an infrared camera. At that time, some phase differences between the temperature pulse and the loading pulse were detected. In the data treatment stage, that phase difference was compensated such that the temperature pulse and the loading pulse were synchronized without time lag.

Table 1.
Material properties of TR330E-150S CFRP laminate used in FEA

Properties	Data	Source
E_1 (GPa)	145	Experiment
E_2 (GPa)	8.31	Experiment
E_3 (GPa)	8.31	Experiment
G_{12} (GPa)	4.88	Experiment
G_{31} (GPa)	4.88	Experiment
G_{23} (GPa)	1.53	Experiment
ν_{12}	0.30	Experiment
ν_{21}	0.02	Experiment
ν_{23}	0.37	Experiment
ν_{32}	0.37	Experiment
ν_{13}	0.30	Experiment
ν_{31}	0.02	Experiment

2.2. Finite Element Analysis

2.2.1. Finite Element Model and Boundary Conditions

The finite model was composed of reduced integration 3-dimensional 20 node elements (C3D20R). Each CFRP layer of 0.125 mm in thickness was modeled with elements of a single element layer, and full-size model of the specimen was analyzed. To give unidirectional properties to each layer, Orientation and Orthotropic options were used. Material properties of Mitsubishi Rayon TR330E-150S with a fiber volume fraction of 70% were used for the FEA (Table 1). Some of the moduli and Poisson ratios were measured by the authors, and others were supplied by Mitsubishi Rayon (Mitsubishi Rayon Co. Ltd, Tokyo, Japan).

The FEA mesh and its boundary conditions are demonstrated in Fig. 3. The one end of the model was constrained not to move along the loading direction, while the opposite end of the model was subjected to a distributed tensile load. Other surfaces were kept constraint-free. Finite element analyses (FEA) were executed using ABAQUS v6.1 in static tensile modes.

2.2.2. Delamination Criterion

With stress distribution results obtained from FEA, we evaluated delamination by the Tsai–Wu failure criterion [15]. The Tsai-Wu failure criterion takes into account the interaction of all six stress components in a quadratic equation. But the main contributors to the delamination are considered to be only the normal stress in the through-thickness direction (σ_z), the shear stress applied in the through-thickness direction on the x plane (τ_{xz}), and the shear stress applied in the through-thickness

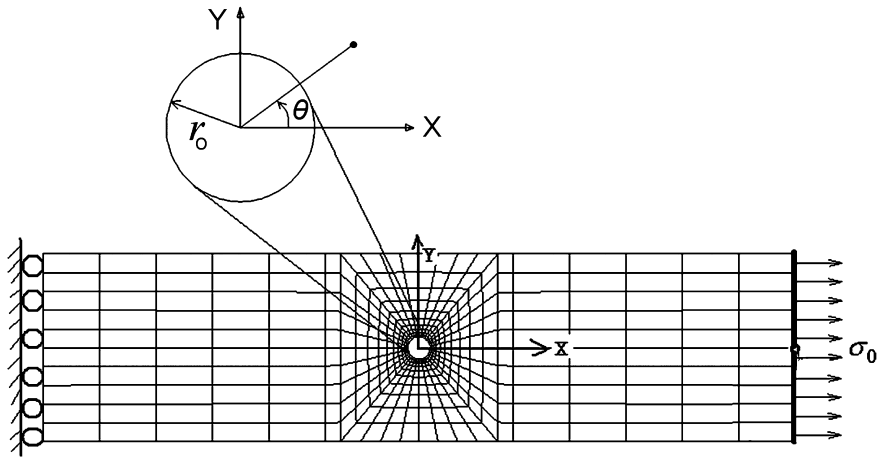

Figure 3. The finite element modeling and the geometric interpretation of a hole.

direction on the y plane (τ_{yz}) [16]. So, the condition for an onset of delamination can be simplified for delamination to give:

$$e^2 = \left(\frac{\tau_{xz}}{F_{xz}}\right)^2 + \left(\frac{\tau_{yz}}{F_{yz}}\right)^2 + \left(\frac{\sigma_z^{\mathrm{t}}}{F_z^{(+)}}\right)^2 + \left(\frac{\sigma_z^{\mathrm{c}}}{F_z^{(-)}}\right)^2 \geqslant 1, \tag{3}$$

$F_z^{(+)}$ and $F_z^{(-)}$ are the tensile and compressive strengths in the thickness direction. F_{yz} and F_{zx} are the transverse shear strengths. e is the delamination indicator, $e \geqslant 1$ corresponding to delamination failure. σ_z^{t} and σ_z^{c} are normal stresses in the thickness-through direction when subjected to tensile and compressive loads, respectively.

Table 2 lists strengths of Mitsubishi Rayon TR330E-150S with a fiber volume fraction of 70%. The strengths, $F_{\mathrm{L}}^{(+)}$ and $F_{\mathrm{T}}^{(+)}$ were measured experimentally by tensile tests, and $F_{\mathrm{TZ}}^{(+)}$ by three-point bending tests [17]. In contrast, the strength $F_{\mathrm{ZT}}^{(+)}$ was estimated by the assumption of transverse isotropy. $F_{\mathrm{L}}^{(-)}$ and $F_{\mathrm{T}}^{(-)}$ were also assumed to be equal to $F_{\mathrm{L}}^{(+)}$ and $F_{\mathrm{T}}^{(+)}$, respectively [18]. Brewer and Lagace's studies also supported the validity of the assumption of transverse isotropy [19]. $F_{\mathrm{Z}}^{(-)}$, the compressive strength along a thickness direction, is generally 3–4 times larger than the tensile stress $F_{\mathrm{L}}^{(+)}$. But when a laminate composite is subjected to a tensile load in the X-direction, the effects of σ_z^{t} and σ_z^{c} on delamination are much smaller than those of other stresses (τ_{iz}). Thereby, we used $F_{\mathrm{Z}}^{(-)}$ as $F_{\mathrm{L}}^{(+)}$. Now, the equation (3) is rewritten as:

$$e^2 = \left(\frac{\tau_{xz}}{F_{xz}}\right)^2 + \left(\frac{\tau_{yz}}{F_{yz}}\right)^2 + \left(\frac{\sigma_z^{\mathrm{t}}}{F_z^{(+)}}\right)^2 + \left(\frac{\sigma_z^{\mathrm{c}}}{F_z^{(+)}}\right)^2 \geqslant 1. \tag{4}$$

Table 2.
Strength of TR330E-150S CFRP laminate

Properties	Data	Source	Properties	Data	Source
$S_L^{(+)}$ (MPa)	2247	Experiment	$S_{LT}^{(+)}$ (MPa)	–	
$S_L^{(-)}$ (MPa)	–		$S_{TL}^{(-)}$ (MPa)	–	
$S_T^{(+)}$ (MPa)	49.7	Experiment	$S_{TZ}^{(+)}$ (MPa)	85	Experiment
$S_T^{(-)}$ (MPa)	–		$S_{ZT}^{(-)}$ (MPa)	85	*Assumption
$S_Z^{(+)}$ (MPa)	49.7	*Assumption	$S_{LZ}^{(+)}$ (MPa)	–	
$S_Z^{(-)}$ (MPa)	49.7	*Assumption	$S_{ZL}^{(-)}$ (MPa)	–	

Note: The S denotes the static strength. Superscripts + and − represent that the strength was measured under tensile mode and compressive mode, respectively. The subscripts L and T represent the longitudinal and transverse directions of CFRP fibers, respectively.

We calculated an average e^2 in an interface along the edge of a hole. The average e^2 on the thickness level of h_i along the angle range (0–θ) was calculated (Fig. 3):

$$e^2|_{z=h_i} = \frac{1}{\theta}\int_0^{\theta} e_{r_0}\,\mathrm{d}\theta. \tag{5}$$

2.3. Evaluation

Stress concentration due to the hole was evaluated with the FEA results. Stress concentration factor (*SCF*) was assigned as the ratio of the maximum stress around the hole to the applied stress:

$$SCF = \frac{\sigma_{\max}}{\sigma_0}. \tag{6}$$

The S–N data from the fatigue tests were logarithmically interpolated as (7). With the logarithmic equations of fatigue specimens, the fatigue strength (S_f) at the target cycle $N = 10^6$ was calculated:

$$\sigma = A + B \cdot \log N. \tag{7}$$

Strength degradation due to a hole was evaluated. The stress degradation ratio (*SDR*) was defined as the difference between ($S_{f,Hole}$) of CFRP specimen with a hole and that without a hole ($S_{f,No\,hole}$) divided by $S_{f,No\,hole}$:

$$SDR(\%) = \frac{(S_{f,No\,hole} - S_{f,Hole})}{S_{f,No\,hole}} \times 100. \tag{8}$$

3. Results and Discussion

3.1. Stress Concentration Around the Hole

Using the stress results obtained from FEA, the stress concentration factor (*SCF*) was calculated as the maximum principal stress at the hole over the externally ap-

plied stress. For isotropic material, $SCF = 3.0$ was expected. $[90_8]$ with a hole was expected to have $SCF = 2.6$ at the middle thickness. $SCF = 5.5$ was predicted on the middle thickness for $[0_8]$. $SCF = 8.8$ was predicted on the interface of 3rd (0°)/4th (90°) layers from the outer surface for $[(0/90)_3]_S$. $SCF = 9.5$ was predicted on the interface of 5th (0°)/6th (45°) layers from the outer surface for $[(0/45/90/-45)_2]_S$. At these four types of CFRP laminates with a hole, the maximum stresses were located in the $\theta = 0°$ direction which passes the center of the hole. $SCF = 5.7$ was predicted on the interface of 1st (45°)/2nd (−45°) layers from the outer surface for $[(\pm 45)_2]_S$. On the interface of 1st (45°)/2nd (45°) layers, the maximum stresses were found at two points on the hole edge. The predicted positions of the maximum stresses in $\theta = 60°$, 150°, 240° and 330° directions for $[(\pm 45)_2]_S$, which coincided with those from reference [20].

SCF of each specimen with a circular notch can be estimated by Whitney–Nuismer stress concentration (K_T) [21]:

$$K_T = K_T^{\infty} \frac{[2 + (1 - d/W)}{3(1 - d/W)}, \tag{9}$$

$$K_T^{\infty} = 1 + [2\sqrt{E_{11}/E_{22} - \nu_{12}} + E_{11}/G_{12}]^{1/2}, \tag{10}$$

K_T^{∞} denotes the stress concentration factor for an infinite plate of orthotropic material. By (14), the $[0_8]$ and $[90_8]$ CFRP laminates commonly having a hole are expected to have $SCF = 9.14$ and $SCF = 2.45$, respectively. The value for $[90_8]$ CFRP laminate by the Whitney–Nuismer equation is matched to the FEA result of the current study. In contrast, that for $[0_8]$ CFRP laminate does not (*SCF* by Whitney–Nuismer = 9.14; *SCF* of our FEA = 5.5). A finite element study also reported that *SCF*s for [0], [90] laminates commonly having a hole were 6.47, 2.5, respectively [22]. Hence, the *SCF* using the Whitney–Nuismer equation cannot be applicable to CFRP laminates having 0° layers.

3.2. Static Strength

$[90_8]$ showed the lowest strength, $[0_8]$ the highest, and the quasi-isotropic laminates showed the middle (Table 3). It can be ordered as following expression:

$$S_t : \begin{array}{c}\text{Specimen}\\ \text{No hole}\\ \text{With a hole}\end{array} = \begin{array}{c}[90_8]\\ 50\text{ MPa}\\ 34\text{ MPa}\end{array} \rightarrow \begin{array}{c}[(\pm 45)_2]_S\\ 226\text{ MPa}\\ 174\text{ MPa}\end{array} \rightarrow \begin{array}{c}[(0/45/90/-45)_2]_S\\ 822\text{ MPa}\\ 621\text{ MPa}\end{array}$$

$$\rightarrow \begin{array}{c}[(0/90)_3]_S\\ 1214\text{ MPa}\\ 790\text{ MPa}\end{array} \rightarrow \begin{array}{c}[0_8]\\ 2247\text{ MPa}\\ 2097\text{ MPa}\end{array}.$$

The strength degradation ratio due to the hole was 35% for $[(0/90)_3]_S$, while the

Table 3.
Results of FEA and experiments

Specimen type	FEA SCF	Static specimen			Fatigue specimen				
		S_t (MPa)	E (GPa)	SDR (%)	f (Hz)	A (MPa)	B (MPa)	S_f at $N = 10^6$ (MPa)	SDR (%)
$[0_8]$		2247 [109]	145	8	–	–	–	–	–
$[0_8]$ with a hole	5.5	2097 [77]	–		–	–	–	–	
$[90_8]$		50 [4]	8.3	32	–	–	–	–	–
$[90_8]$ with a hole	2.6	34 [1]	–		–	–	–	–	
$[(\pm45)_2]_S$		226 [6.6]	16.1	23	–	–	–	–	–
$[(\pm45)_2]_S$ with a hole	5.7	174 [7]	–		–	–	–	–	
$[(0/45/90/-45)_2]_S$		822 [12]	55.9	24	5	759	−20	639	9 (5 Hz)
					10	849	−29	675	22 (10 Hz)
$[(0/45/90/-45)_2]_S$ with a hole	9.5	621 [19]	–		5	687	−18	579	
					10	648	−19	528	
$[(0/90)_3]_S$		1214 [34]	75.3	35	5	1314	−22	1180	11 (5 Hz)
					10	1361	−24	1220	25 (10 Hz)
$[(0/90)_3]_S$ with a hole	8.8	790 [23]	–		5	1225	−30	1050	
					10	979	−11	913	

Note: The SCF and SDR present the stress concentration factor and the strength ratio, respectively. The E denotes the Young's modulus. The f denotes the frequency of cycling loads. The A and B are constants of the logarithmically interpolated equation ($\sigma = A + B \log N$) of S–N curve. The S_t and S_f present the tensile strength of static specimens and the allowable tensile strength of fatigue specimen at $N = 10^6$, respectively. The numbers inside [] in the S_t column present the standard deviation.

minimum degradation was 8% for $[0_8]$ (Table 3):

$$SDR\ (\text{static specimens}) : \frac{[0_8]}{8\%} \rightarrow \frac{[(\pm45_2]_S}{23\%} \rightarrow \frac{[(0/45/90/-45)_2]_S}{24\%} \rightarrow \frac{[90_8]}{32\%} \rightarrow \frac{[(0/90)_3]_S}{35\%}.$$

Static and fatigue strengths of fiber-reinforced composites with a open hole notch have been predicted by the Whitney–Nuismer average stress model [7, 8]:

$$\frac{S_{hole}}{S} = \frac{K_T^{\infty}}{K_T}\left(\frac{S_{hole}}{S}\right)^{\infty}, \tag{11}$$

$$\frac{S_{hole}^{\infty}}{S} = 2[2 + 2x + x^2 + x^3 + (K_T^{\infty} - 3)x^6(1 + x)]^{-1}, \tag{12}$$

where $x = d/(d + 2\alpha_0)$, and α_0 is the characteristic distance. The *SDR*s predicted by the Whitney–Nuismer average stress model were larger than our experimental data. The *SDR*s of $[0_8]$ and $[90_8]$ CFRP laminates commonly having a hole are expected as 47% and 44% by the Whitney–Nuismer average stress model, respectively. Compared with our experimental results, i.e. $SDR = 8\%$ and $SDR = 32\%$ for

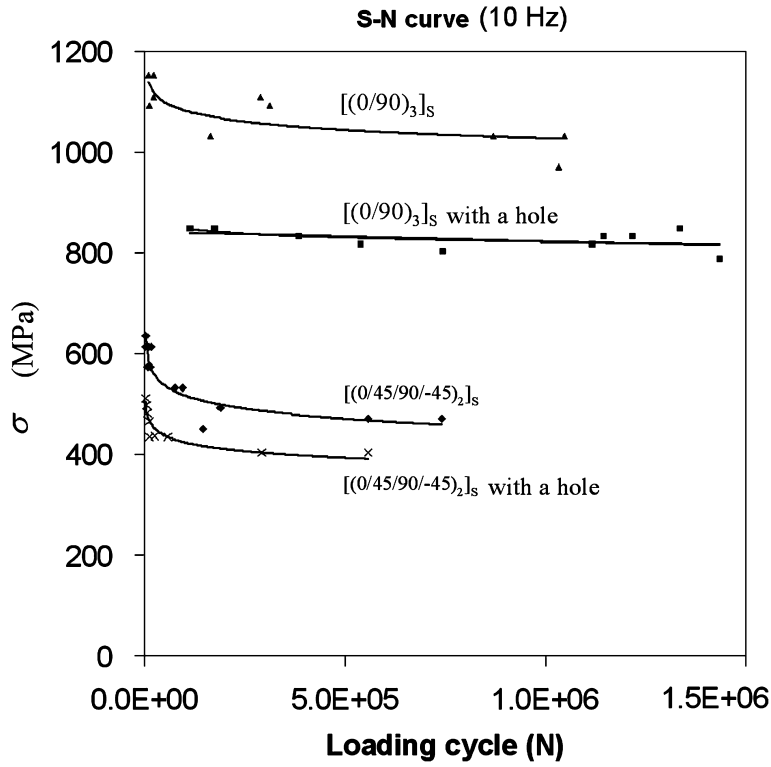

Figure 4. S–N curve of fatigue tests performed under the frequency of 10 Hz.

$[0_8]$ and $[90_8]$ CFRP laminates having a hole, the *SDR*s predicted by the Whitney–Nuismer average stress model are much larger.

3.3. Fatigue Strength

The allowable fatigue strengths (S_f) for a target loading cycle of $N = 10^6$ was calculated using $\sigma = A + B \cdot \log N$ (Fig. 4 and Table 3). Figure 4 demonstrates the S–N curve of quasi-isotropic CFRPs and cross-ply CFRPs tested under fatigue frequency $f = 10$ Hz. The failure strength decreased with increased loading cycle. Twelve-layered cross-ply CFRPs had higher strength than 16-layered quasi-isotropic CFRPs, and the specimens with a hole showed lower strengths. In the cases of CFRP specimens without a hole, S_f of each specimen was evaluated in the next order:

$$S_f : \frac{\text{Specimen}}{\text{No hole}} = \frac{[(0/45/90/-45)_2]_S}{639\ \text{MPa (5 Hz)}} \rightarrow \frac{[(0/45/90/-45)_2]_S}{675\ \text{MPa (10 Hz)}} \rightarrow \frac{[(0/90)_3]_S}{1180\ \text{MPa (5 Hz)}} \rightarrow \frac{[(0/90)_3]_S}{1220\ \text{MPa (10 Hz)}}.$$

In contrast, in the fatigue specimens with a hole, the allowable fatigue strength at $N = 10^6$ decreased about 10% for both $[(0/45/90/-45)_2]_S$ and $[(0/90)_3]_S$ as the

loading frequency changed from 5 Hz to 10 Hz. The hole caused the strengths of $[(0/90)_3]_S$ and $[(0/45/90/-45)_2]_S$ to degrade by 9% and 11% under 5 Hz loading frequency, respectively, and by 22% and 25% under 10 Hz loading frequency, respectively:

$$SDR \text{ (fatigue specimens)} : \frac{[(0/90)_3]_S}{\begin{matrix}9\%\ (5\ \text{Hz}) \\ 22\%\ (10\ \text{Hz})\end{matrix}} \rightarrow \frac{[(0/45/90/-45)_2]_S}{\begin{matrix}11\%\ (5\ \text{Hz}) \\ 25\%\ (10\ \text{Hz})\end{matrix}}.$$

By the Whitney–Nuismer average stress model and $\alpha_0 = 1.25$ [23], it was reported that there was $SDR = 37\%$ in static strength of $[(45/0/-45/90)_4]_S$ with a hole of $d/W = 0.199$ and $SDR = 30$–40% in static strength of a quasi-isotropic CFRP laminate with a hole of $d/W = 0.167$ [8]. Hence, the *SDR* calculation by the Whitney–Nuismer average stress model is considered to overestimate the stress degradation due to a hole.

3.4. Fatigue Processes of the Fatigue Specimens with the Hole

Figures 5 and 6 demonstrate fatigue failure processes and infrared images of the tested fatigue specimens. Figures 5(a) and 6(a) describe the schemes of the failure process that were reconstructed based on real observation of the fatigue tests. Figures 5(b) and 6(b) represent infrared stress images at several fatigue cycles. On the infrared images (see online version in color), the color spectrum from cold to hot colors indicates various stress conditions: black (empty space or out of detection) → blue (compressive stress) → white (near to stress zero) → green (middle stress) → yellow (high stress) → red (very high stress).

Figure 5(a) and 5(b) show the fatigue failure processes and the infrared stress images of $[(0/45/90/-45)_2]_S$ with a hole. Figure 5(a) represents that failure initiated near the hole, then delamination starts at extreme free edges in the width direction, and a through-width breakage occurred first in the outer-most layer (0° layer). The infrared images (Fig. 5(b)) show that initial high stresses occurred at the left-most and right-most edges (when $N = 1700$), and they induced delaminatinon at the those edges ($N = 30\,000$). Even though the existence of any high stress is not noticeable, a failure is also observed around the hole ($N = 30\,000$). The failures on the outer-most layer propagate along the width direction ($N = 85\,000$). The infrared images showing the failures of other layers are not shown ($N > 85\,000$).

Figure 6(a) and 6(b) shows the fatigue failure processes and the infrared stress images of $[(0/90)_3]_S$ with a hole. Figure 6(a) demonstrates that a failure initiated around the edge of the hole. Through-thickness failures were observed in the 90° layers and the polymer matrixes of the 0° layers. Even after all the 90° layers and the polymer matrix of the 0° layers were failed, the carbon fibers in the 0° layers still survived. Figure 6(b) shows the infrared stress images of $[(0/90)_3]_S$ with a hole at several loading cycles. High stresses are distributed bilaterally with respect to the hole ($N = 2000$). With further deformation, the stress image at $N = 12\,700$ shows colder colors than those at $N = 2000$ because the heat of inner layers is

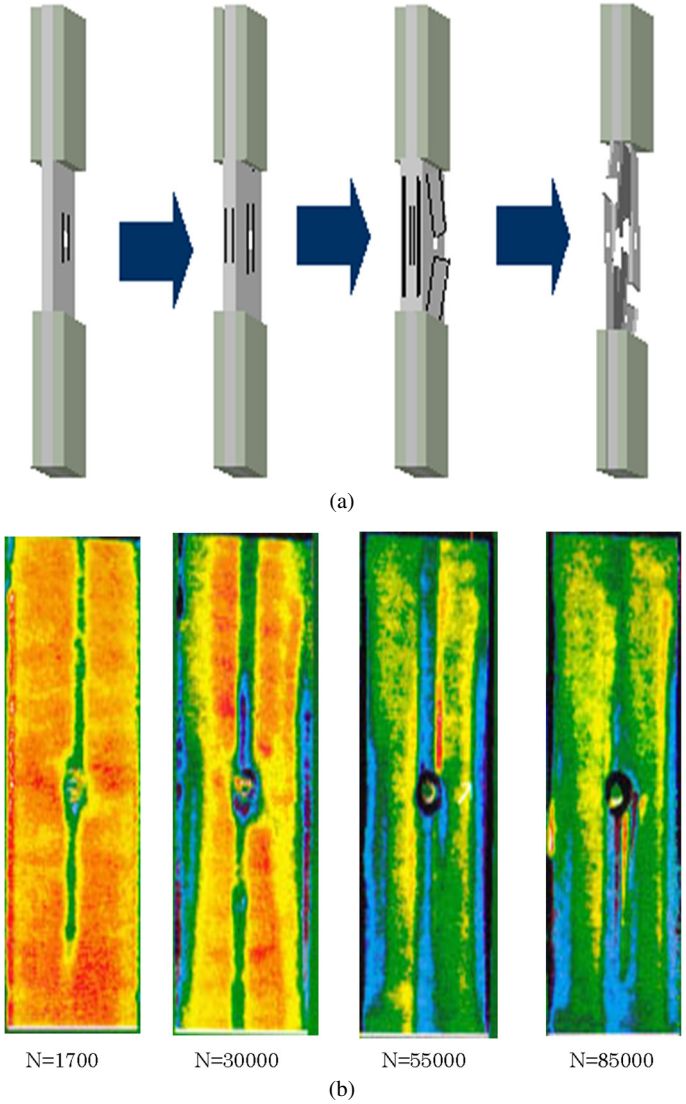

Figure 5. Fatigue process of $[(0/45/90/-45)_2]_S$ with a hole. This figure is published in color on http://www.ingentaconnect.com/content/vsp/acm

not transferred to the outermost layer due to delamination at 0°/90° interface and breakages of 90° layers. As it deforms, stress is concentrated at the lateral edges of the hole ($N = 410\,000$). Then there is a large longitudinal elongation of hole at $N = 1\,223\,200$ before through-thickness breakage of plastic matrix.

3.5. Delaminations in Fatigue Tests

Figure 7(a) and 7(b) show the delamination index of $[(0/45/90/-45)_3]_S$ with a hole by FEA and an ultrasonic image, respectively. Figure 7(a) shows the FEA results

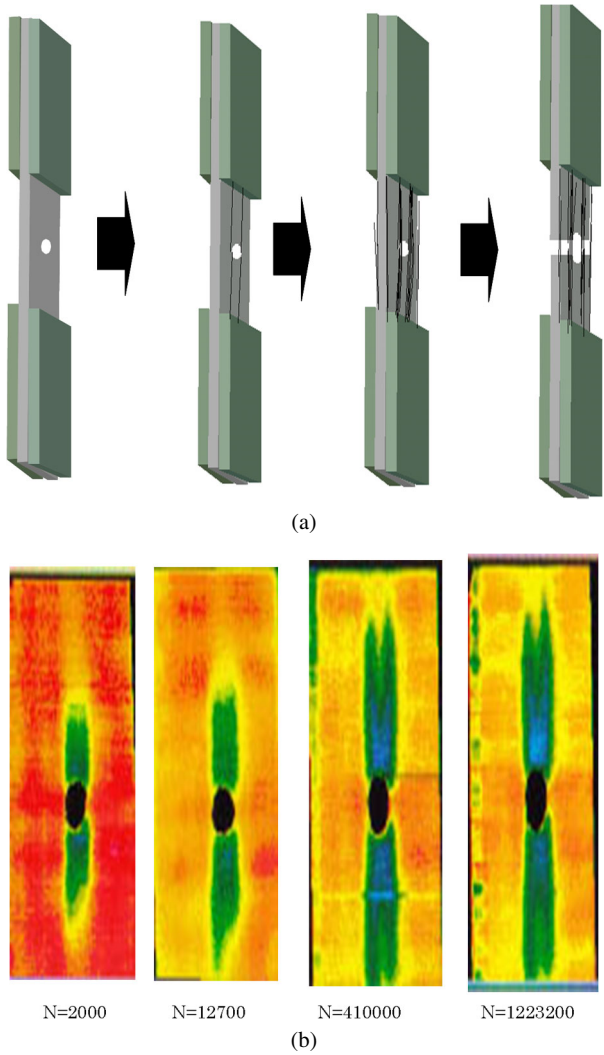

Figure 6. Fatigue process of $[(0/90)_3]_S$ with a hole. This figure is published in color on http://www.ingentaconnect.com/content/vsp/acm

that a primary delamination position is predicted to occur in the 1st interface from the outer surface. In the actual fatigue tests, the earliest delamination was observed in the 1st interface from the outermost layer. Figure 7(b) is the ultrasonic images $[(0/45/90/-45)_3]_S$ specimen with a hole after the loading cycle, $N = 10^6$. The red color indicates failure. In the ultrasonic image, a large portion of red color is located around the level of 0.35 mm from the outmost surface which corresponds to the 3rd interface from the outermost surface, i.e. between 90° and −45° layers. The depth of the 3rd interface should be 0.375 mm before deformation. It might decrease, however, after tensile fatigue loadings.

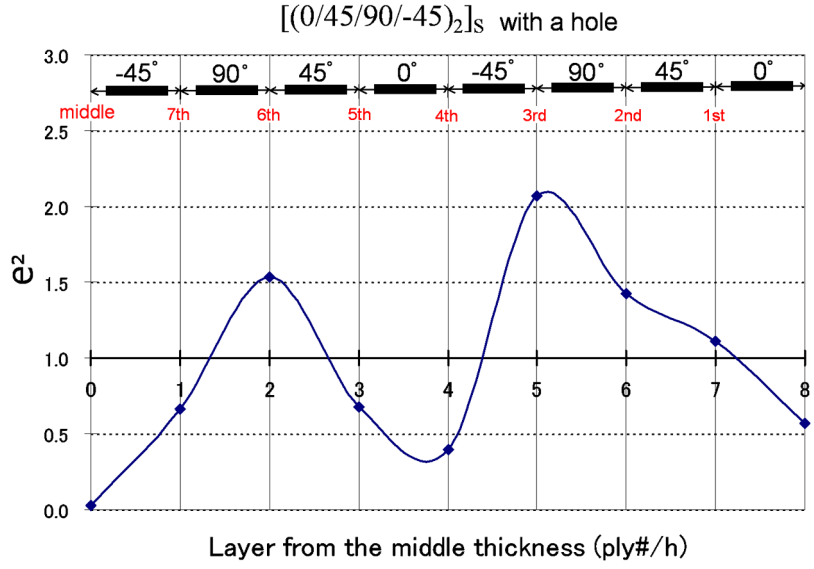

(a)

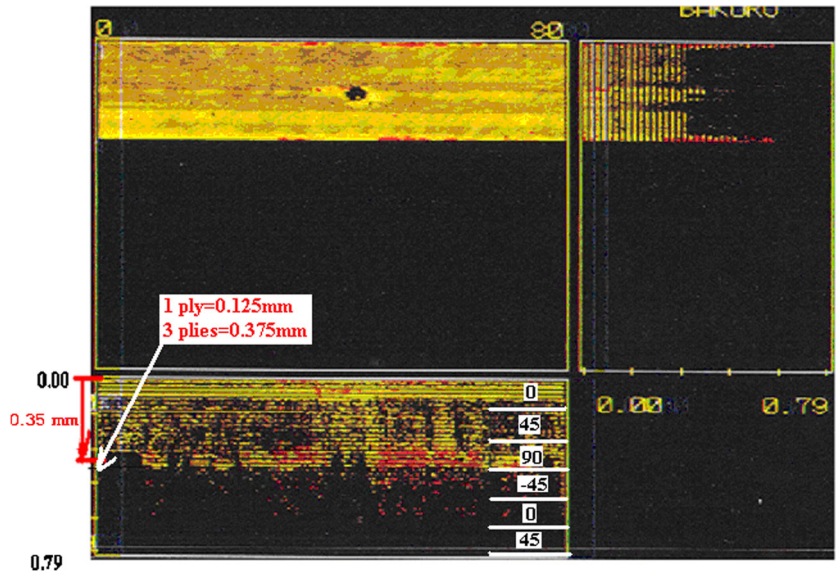

(b)

Figure 7. Delamination evaluation around the edge of a hole in $[(0/45/90/-45)_2]_S$ with a hole. This figure is published in color on http://www.ingentaconnect.com/content/vsp/acm

Figure 8(a) and 8(b) shows the delamination index of $[(0/90)_3]_S$ with a hole by FEA and an ultrasonic image, respectively. In the FEA results, two main delamination positions were predicted in the 1st and 5th interfaces (Fig. 8(a)). Figure 8(b) shows an ultrasonic image that scanned failure through the specimen of $[(0/90)_3]_S$ specimen with a hole after the fatigue cycle of $N = 3000$ (see online version in

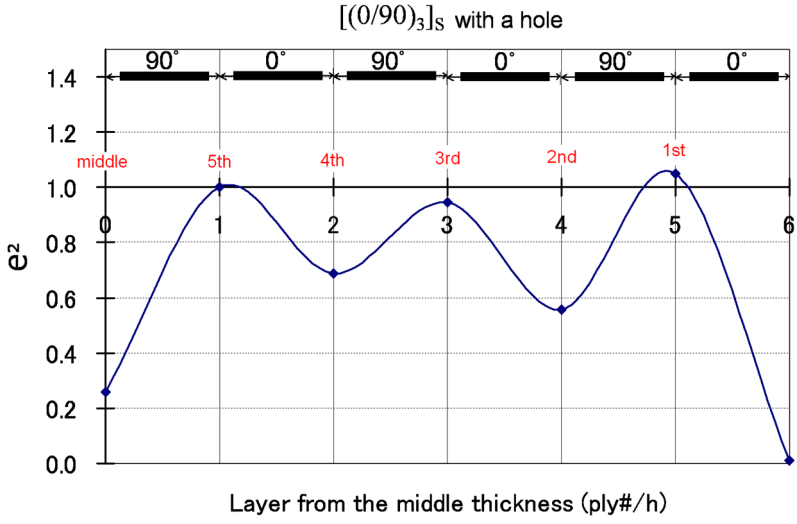

(a)

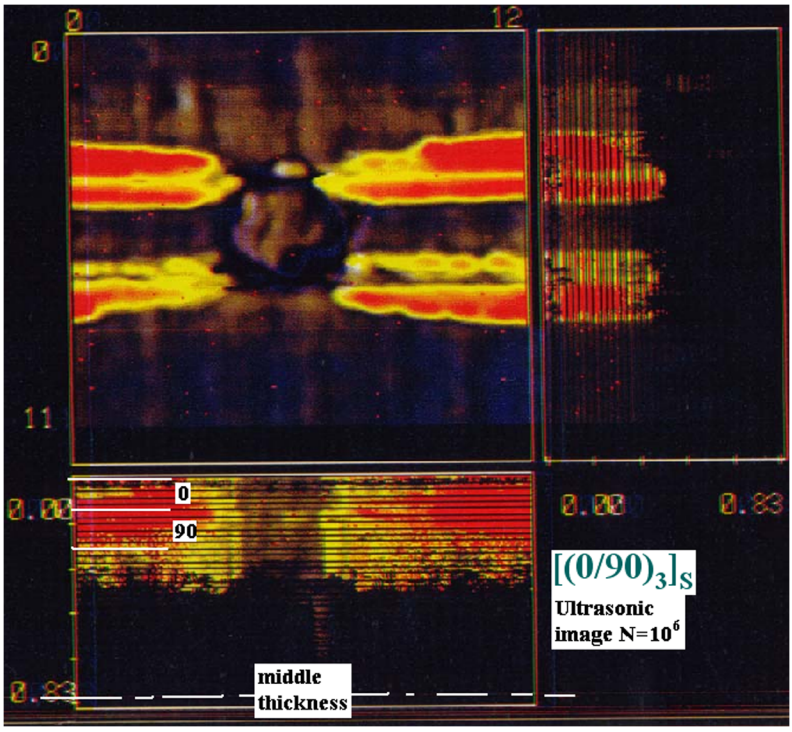

(b)

Figure 8. Delamination evaluation around the edge of a hole in $[(0/90)_3]_S$ with a hole. This figure is published in color on http://www.ingentaconnect.com/content/vsp/acm

color). The red color indicates failure. Large red areas were observed in the thickness of 0.1–0.2 mm in depth. This thickness level corresponds to the 1st interface and the 1st 90° layer from the outermost surface, since each layer might have slightly smaller thickness than the intact thickness of 0.125 mm. The failure at the 5th interface was not detected using the ultrasonic imaging system since the depth 0.6 mm of the 5th interface was beyond detectable range.

4. Conclusions

The current study assessed the effect of a bolt hole on the fatigue properties of CFRP laminates. The tested specimens were $[(0/90)_3]_S$, $[(0/45/90/-45)_2]_S$, $[0_8]$, $[90_8]$ and $[(\pm 45)_2]_S$ laminates with or without a hole. A hole whose diameter corresponds to 0.12 times the specimen width caused the fatigue strength to decrease by 9% and 11% under 5 Hz loading frequency, and by 22% and 25% under 10 Hz loading frequency for $[(0/90)_3]_S$ and $[(0/45/90/-45)_2]_S$, respectively. Because the decrease in cross-sectional area due to the hole was normalized in calculation of the tensile strength, a stress concentration around the hole is believed to induce the strength degradation of fatigue specimens. From the finite element analyses, the stress concentration factor around a hole was expected as 8.8 and 9.5 for $[(0/90)_3]_S$ and $[(0/45/90/-45)_2]_S$, respectively. By using an infrared image system, the failure of $[(0/45/90/-45)_2]_S$ could be *in situ* monitored, and the primary delamination occurred in an outer interface (90/−45).

The delamination positions predicted by FEA results were well matched to the experimental results.

4.1. Conflict of Interest Statement

None of the authors of this manuscript has received or will receive any type of support, funding, or benefits for personal or professional use from a commercial party related directly or indirectly to the subject of this article.

References

1. Y. Hamaguchi and T. Shimokawa, Fatigue Strength of Open Hole Specimens of a T800H/PMR-15 Carbon/Polyimide Composite, Technical Report of National Aerospace Laboratory NAL TR-1392 (1999).
2. F. Z. Hu, C. Soutis and E. C. Edge, Interlaminar stresses in composite laminates with a circular hole, *Compos. Struct.* **37**, 223–232 (1997).
3. S. Sihn, R. Y. Kim, K. Kawabe and S. W. Tsai, Experimental studies of thin-ply laminated composites, *Compos. Sci. Technol.* **67**, 996–1008 (2007).
4. J. Senthilvasan, D. P. Thambiratnam and G. H. Brameld, Dynamic response of a curved bridge under moving truck load, *Engng Struct.* **24**, 1283–1293 (2002).
5. M. R. Kharrazi and S. Sarkani, Frequency-dependent fatigue damage accumulation in fiber-reinforced plastics, *J. Compos. Mater.* **35**, 1924–1953 (2001).
6. S. C. Tan, Laminated composites containing an elliptical ppening. II. Experiment and model modification, *J. Compos. Mater.* **21**, 949–968 (1987).

7. N. Tsangarakism, J. M. Slepetz and J. Nunes, Static and fatigue notch strength prediction in alumina fiber reinforced aluminium plates with a circular hole, *J. Compos. Mater.* **22**, 386–393 (1988).
8. T. Shimokawa, Y. Kakuta, Y. Hamaguchi and T. Aiyama, Static and fatigue strengths of a G40-800/5260 carbon fiber/bismaleimide composite material at room temperature and 150°C, *J. Compos. Mater.* **42**, 655–679 (2008).
9. C. Scarponi and G. Briotti, Ultrasonic technique for the evaluation of delaminations on CFRP, GFRP, KFRP composite materials, *Composites Part B: Engng* **31**, 237–243 (2000).
10. S. Yashiro, J. Takatsubo and N. Toyama, An NDT technique for composite structures using visualized Lamb-wave propagation, *Compos. Sci. Technol.* **67**, 3202–3208 (2007).
11. K. Kurashiki, Q. Q. Ni and M. Iwamoto, Fatigue damage evaluation of GFRP using infrared thermography — effects of matrix resin and fiber content on evaluation of fatigue damage, *Zairyo/J. Soc. Mater. Sci., Japan* **52**, 1253–1257 (2003).
12. S. Sugimoto and T. Ishikawa, Numerical analysis of heat conduction effect corresponding to infrared stress measurements in multi-lamina CFRP plates, *Adv. Compos. Mater.: Official J. Japan Soc. Compos. Mater.* **8**, 269–279 (1999).
13. R. Steinberger, T. I. Valadas Leitao, E. Ladstatter, G. Pinter, W. Billinger and R. W. Rang, Infrared thermographic techniques for non-destructive damage characterization of carbon fibre reinforced polymers during tensile fatigue testing, *Intl J. Fatigue* **28**, 1340–1347 (2006).
14. L. Toubal, M. Karama and B. Lorrain, Damage evolution and infrared thermography in woven composite laminates under fatigue loading, *Intl J. Fatigue* **28**, 1867–1872 (2006).
15. S. W. Tsai and E. M. Wu, A general theory of strength for anisotropic materials, *J. Compos. Mater.* **5**, 58–80 (1971).
16. J. P. Hou, N. Petrinic and C. Ruiz, A delamination criterion for laminated composites under low-velocity impact, *Compos. Sci. Technol.* **61**, 2069–2074 (2001).
17. G. Ben, Y. Tanimoto and M. Hashimoto, Transverse shear properties of CFRP laminates under static loading, *Zairyo/J. Soc. Mater. Sci., Japan* **47**, 287–292 (1998).
18. R. Y. Kim and S. L. Donaldson, Experimental and analytical studies on the damage initiation in composite laminates at cryogenic temperatures, *Compos. Struct.* **76**, 62–66 (2006).
19. J. C. Brewer and P. A. Legace, Quadratic stress criterion for initiation of delamination, *J. Compos. Mater.* **22**, 1141–1155 (1988).
20. C. S. Hong and J. H. Crews, Jr., Stress concentration factors for finite orthotropic laminates with a circular hole and uniaxial loading, NSA TP-1469 (1979).
21. R. J. Nuismer and J. M. Whitney, Uniaxial failure of composite laminates containing stress concentrations, *ASTM STP* **593**, 117–142 (1975).
22. C. S. Hong, Stress concentration factors for finite orthotropic graphite/E laminate with a circular hole, *Trans. Korean Soc. Mech. Engrs* **4**, 113–118 (1980).
23. N. Tsangarakis, Fatigue failure of an orthotropic plate with a circular hole, *J. Compos. Mater.* **18**, 47–57 (1984).